Physics-based modelling of wind-driven junction fires

This is the Published version of the following publication

Physics-based modelling of wind-driven junction fires

Ahmad Hassan [a,*], Gilbert Accary [b], Duncan Sutherland [c], Khalid Moinuddin [a]

[a] *Institute for Sustainable Industries and Liveable Cities, Victoria University, Melbourne, VIC, 8001, Australia*
[b] *School of Engineering, Lebanese American University, PO Box: 36, Byblos, Lebanon*
[c] *School of Science, University of New South Wales, PO Box 7916, Canberra BC, ACT, 2610, Australia*

ARTICLE INFO

ABSTRACT

Numerical simulations of laboratory-scale junction fires were performed for a shrub fuel bed, using the fully-physical model FIRESTAR3D under various unidirectional wind conditions on different terrain slopes and junction angles. Simulations were carried out for a junction angle ranging from 15° to 90°, for a slope angle varying between 0 and 40°, and for low to intermediate driving wind speed, ranging from 0 to 4 m/s. Simulations show surge-and-stall-like behaviour of fire spread that is irregularly enhanced by the action of wind. Results of fire spread show that the effect of the junction angle on fire behaviour is non-linear, becoming stronger as the angle decreases. Both wind and slope effects are concealed by the junction effect for small angles, while wind has a significant impact at intermediate values of the junction angle. The driving heat transfer mode in junction fires varies based on the slope condition: on sloping terrain, convection is dominant for any wind speed, while on non-sloping terrain, radiation is the driving mode in no-wind condition but convection plays the greater role as the wind speed increases.

1. Introduction

Even though the number of extreme fire events is relatively small, the amount of damage caused by them is enormous [1,2]. Nevertheless, these events are increasing as a consequence of climate change and other human activities such as large-scale urbanisation in wildlands and the reduction of agricultural areas. Extreme fire events are characterised by unpredictable propagation, excessive heat release rates (HRR), and exceptionally high rates of fire spread (ROS) and fire line intensity [3], where wind channelling ways can play a major role in exacerbating the situations.

Wind is well-known as one of the main factors that increase the spread of wildfire. It does so due to elongated flame spreading over drier virgin fuel, and increasing heat flux and pyrolysis. Wildfires often exhibit complex and dynamic behaviour arising from interactions between the fire and surrounding atmospheric and terrain conditions (such as wind, ground slope etc.) that can create a rapid fire–advancement, resulting in a loss of containment, properties and human lives.

The intersection of two fire fronts (known as junction fire) is a form of extreme fire behaviour and is characterised by a relatively high speed of propagation caused by strong interactions between the two fronts [4–6]. A detailed literature review on junction fire was presented in Hassan et al. [7], where a parametric study was conducted using the physics-based model FIRESTAR3D [8] after a validation study [9]. The current paper is an extension of these investigations and aims to examine the combined effect of wind speed (U) and ground slope angle (α) on the junction fire propagation and behaviour for various junction angles (θ). Fig. 1 shows the ideal case of a junction fire considered in this study, as well as the parameters that are being investigated.

Sullivan et al. [10] conducted small-scale experiments involving junction fires within a wind tunnel, with a maximum fire line length of 1.5 m. The authors found an increase in the ROS for wind-driven conditions, considerably greater than what could be explained by geometric effects alone (junction effect). Filkov et al. [11] conducted field experiments under some prevailing wind which was inconsistent in directions and speeds. In terms of propagation behaviour, the results of the experiments in wind-driven conditions agreed with the results of Sullivan et al. [10]. Again, the increase in the rate of propagation of the junction point was found to be above what would be expected from the geometric effect alone for all junction fire fronts.

The computational fluid dynamics (CFD) code "FIRSTAR3D" [8] used in this work is a three-dimensional physics-based fire model [9,12]
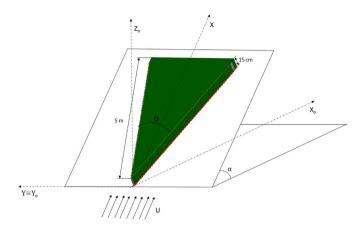
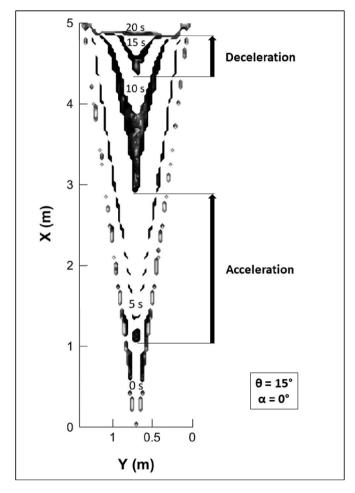**Fig. 1.** Illustration of the vegetation layer in V-shape on a slope with wind acting in X-direction.

Fig. 2. Evolution of fire perimeter based on the pyrolysis front showing propagation phases. The first perimeter corresponds to the initial state and the time difference between two consecutive perimeters is 5 s.

that is based on a multi-phase formulation. The model consists of the conservation equations of the coupled system formed by the vegetation and the surrounding gaseous medium. The model considers the different chemical processes occurring in the vegetation (drying, pyrolysis, and combustion), the different transport mechanisms and phenomena occurring in the surrounding gaseous phase (convection, radiation, turbulence, combustion …), and the interaction between the fluid and the solid phases (aerodynamic drag, heat transfer by convection and

radiation, and mass transfer).

FIRESTAR3D has been extensively validated [9,12–14]. Frangieh et al. [13] performed simulations of fire propagation under various conditions, including small- and large-scale experiments conducted respectively inside a wind tunnel (with wind speeds ranging from 0.22 to 0.89 m/s) and in the field (with wind speeds ranging from 1 to 16 m/s). The results of these simulations exhibited good agreement with the corresponding experimental data and with the predictions of other models. Fayad et al. [14] presented fire experiments and FRESTAR3D simulations conducted on sloped terrains covered by dense shrubland vegetation. Good agreements between the experimental data and the numerical results were obtained in terms of the shape of the fire front, as well as in terms of the radiant and total heat fluxes received at different targets.

This series of investigations, involving junction fire, slope and wind, started with the validation conducted by Hassan et al. [9] against the ROS measurement of laboratory-scale junction fires conducted by Raposo et al. [6]. The numerical model replicated the experimental set-up, captured the correct order of magnitude of the ROS, and showed well-aligned agreement for different qualitative features of the fire. Hassan et al. [7] conducted a parametric study with various combinations of junction angles and slope angles with no applied wind. It was found that acceleration and deceleration phases appear for a small junction angle depending on the slope angle (see Fig. 2). The junction angle of 45° was found to be the threshold value beyond which the deceleration phase was no longer observed. Fire propagation for high junction angles accelerates slightly before becoming steady. For low junction angles, the deceleration phase is only evident in no-slope conditions, where the junction angle undergoes a significant increase. The vegetation receives energy by convection more than by radiation in steep-slope cases, while the vegetation loses more heat by convection than by radiation in no-slope conditions.

The present investigation builds upon the previous ones [7,9], as well as other validation studies conducted with the FIRESTAR3D model under windy and sloped conditions. In this work, the objective is to investigate the impact of driving wind speed, combined with slope, on the propagation of junction fires at various junction angles.

2. Numerical modelling

A detailed description of FIRESTAR3D was given in Ref. [7]; therefore, it is only briefly discussed in this paper.

2.1. Model description

FIRESTAR3D model consists of fundamental conservation equations of mass, momentum, and energy within discrete control volumes encompassing both a solid phase (vegetation) and a fluid phase (surrounding gases). This formulation requires the introduction of source and sink terms into the equations, representing interactions between the two phases, such as mass exchange, drag, and heat exchange by means of convection and radiation. The FIRESTAR3D model is structured into two distinct parts that are separately addressed on their respective grids. The first part solves the equations governing a turbulent and reactive flow in the gaseous phase, where fresh air chemically reacts with gaseous products resulting from vegetation degradation processes (drying and pyrolysis) and combustion. The second part solves the equations governing the state and composition of the vegetation, exposed to the intense heat flux originating from the flaming zone.

The conservation equations for mass, momentum, energy (in enthalpy formulation), and chemical species (O_2, N_2, CO, CO_2, and H_2O) are solved using a large eddy simulation (LES) approach (Smagorinsky sub-grid-scale model with $C_{SGS} = 0.07$). Combustion in the fluid phase is modelled using the Eddy Dissipation Concept (EDC). Radiative heat transfer, which is an essential mechanism that drives fire front propagation, is computed using the Discrete Ordinate Method (DOM) [7,8].
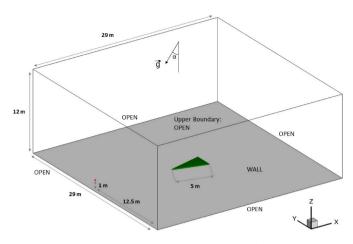
Fig. 3. Perspective view showing the computational domain, the V-shape vegetation cover, and the applied boundary conditions.

Details of the solid fuel and fluid-phase combustion modelling can be found in the paper appendix.

2.2. Simulation parameters

Numerical simulations were carried out using V-shaped vegetation immersed inside a larger computational domain (29 m long, 29 m wide, and 12 m high), as shown in Fig. 3. Open boundary conditions were imposed on all computational domain sides except its bottom where a solid-wall condition was applied. A homogeneous junction fuel bed, of height 0.15 m and junction edges' length 5 m, was located 12 m away from the lateral boundaries. The simulations were carried out for a fuel moisture content of 20%. The thermo-physical properties of the shrub fuel layer are given in Table 1. Solid-fuel particles were assumed to have a cylindrical shape and to behave as a black body with a drag coefficient

$C_D = 0.42$ [15]. A uniform mesh with ($\Delta x, \Delta y, \Delta z$) = (0.025 m, 0.025 m, 0.0125 m) was used for the solid phase, while a non-uniform grid of $160 \times 160 \times 160$ cells was used for the fluid one. Within the vegetation zone, the fluid-phase grid was uniform with ($\Delta x, \Delta y, \Delta z$) = (0.05 m, 0.05 m, 0.025 m) and then the fluid-phase grid was gradually coarsened toward the open boundaries according to a geometric progression. Both the solid-phase and the fluid-phase grids are characterised by cell sizes below the extinction radiation length scale [16] within the vegetation given by $\frac{4}{\alpha_S \sigma_S}$ and equals to 0.073 m in our case. To avoid false fire extinction, this value should not be exceeded, especially in the case of radiation-dominated fire. This configuration was extensively tested through sensitivity analyses for grid size, computational domain size, and other numerical parameters [9]; the results consistently demonstrated the results independence of these parameters. The domain inclination angle to the Earth horizontal, α, was specified through the angle between Earth gravitational acceleration and the z-coordinate direction of the computation domain. Consequently, the gravitational acceleration has two non-zero components: $g_x = -g\sin(\alpha)$ and $g_z = -g\cos(\alpha)$, where $g = 9.81$ m/s^2 is acceleration due to Earth gravity.

Before ignition, the hydrodynamic module of the code was run for 30 s to ensure the development of the turbulent flow inside and above the vegetation. Then, the fire lines were ignited in the model by activating a simulated gas burner. At $t_{ignition} = 30$ s, a 10-cm wide burner was activated along the entire ignition lines by injecting CO gas at 1600 K from the bottom of the computational domain for the duration of 5 s.

By analogy to the method used in Hassan et al. [7,9], the fire front was tracked by examining the mass fraction of dry vegetation and identifying the pyrolysis front. The overall advancement of the fire front in the simulations was determined by analysing the distribution of dry material mass fraction: the fire front located on areas where the fuel bulk density ($\alpha_S \rho_S$) reaches a threshold of 0.001 kg/m^3).

In FIRESTAR3D, the prevailing wind speed is applied by a pressure gradient between the inlet and outlet, that maintains wind velocity constant at a specified point of the computational domain (usually a

Table 1
Geometric and physical properties of the shrubland vegetation [6,15].

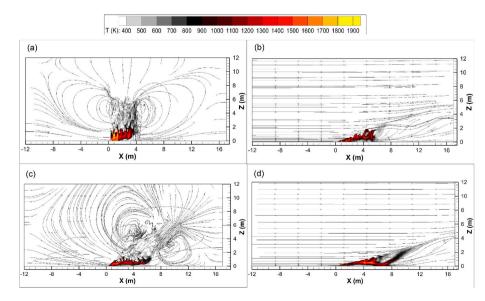| Vegetation height (m)	Solid-fuel volume fraction α_s	Surface/Volume ratio σ_s (m^{-1})	Dry material density ρ_S (kg.m^{-3})	Drag Coefficient C_D	Thermal emissivity	Vegetation family shape
0.15	0.00784	6900	500	0.42	1	Cylindrical

Fig. 4. Temperature fields and streamlines obtained numerically at t − tignition = 6 s in the vertical median xz plane (passing through the junction point) for a junction angle $\theta = 15°$. (a) $\alpha = 0°$, $U = 0$ m/s; (b) $\alpha = 0°$, $U = 4$ m/s; (c) $\alpha = 40°$, $U = 0$ m/s; and (d) $\alpha = 40°$, $U = 4$ m/s.
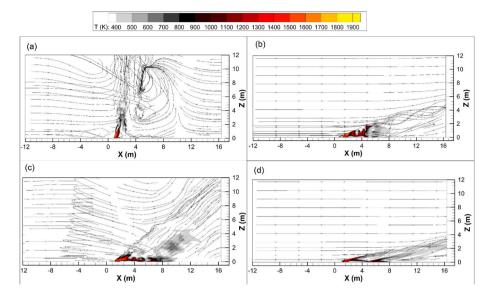
Fig. 5. Temperature fields and streamlines obtained numerically at $t - t_{ignition} = 15$ s in the vertical median xz plane (passing through the junction point) for a junction angle $\theta = 60°$. (a) $\alpha = 0°$, $U = 0$ m/s; (b) $\alpha = 0°$, $U = 4$ m/s; (c) $\alpha = 40°$, $U = 0$ m/s; and (d) $\alpha = 40°$, $U = 4$ m/s.

Fig. 6. Time evolutions of the average junction point position (AJPP) and of the dynamic ROS obtained for $\theta = 15°$ (a to c) and for $\theta = 30°$ (d to e), and different combinations of the slope angle and wind speed. Recall the used notation: S1520V2 corresponds to a simulation with $\theta = 15°$, $\alpha = 20°$, and $U = 2$ m/s. The horizontal solid line corresponds to the average ROS.

point where wind is not perturbed by the presence of fire), and the velocity profile at the inlet boundary is determined from mass conservation [8]. In this work, the pressure gradient is applied in the x-direction and the velocity was maintained at point (X = 0, Y = 14.5 m, Z = 1 m)

shown in Fig. 3.

The parametric study focuses on the influence of open wind speed on fire behaviour in terms of ROS, HRR and modes of heat transfer. The simulations were carried out for slope angles ranging from 0° to 40°
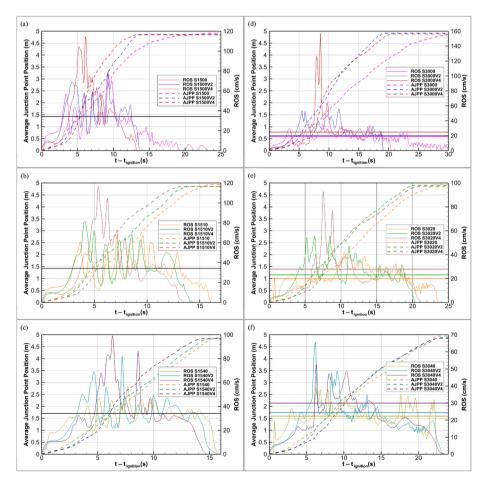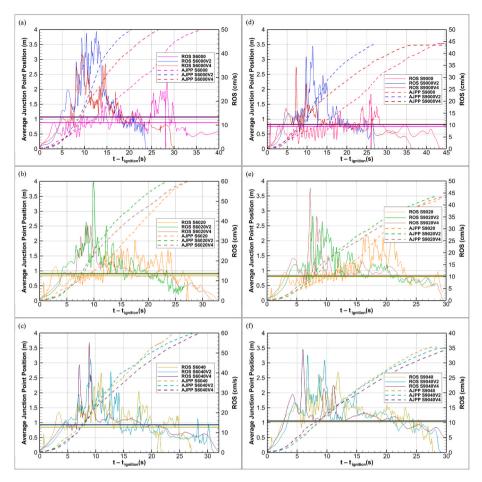
Fig. 7. Time evolutions of the average junction point position (AJPP) and of the dynamic ROS obtained for $\theta = 60°$ (a to c) and for $\theta = 90°$ (d to e), and different combinations of the slope angle and wind speed. Recall the used notation: S1520V2 corresponds to a simulation with $\theta = 15°$, $\alpha = 20°$, and $U = 2$ m/s. The horizontal solid line corresponds to the average ROS.

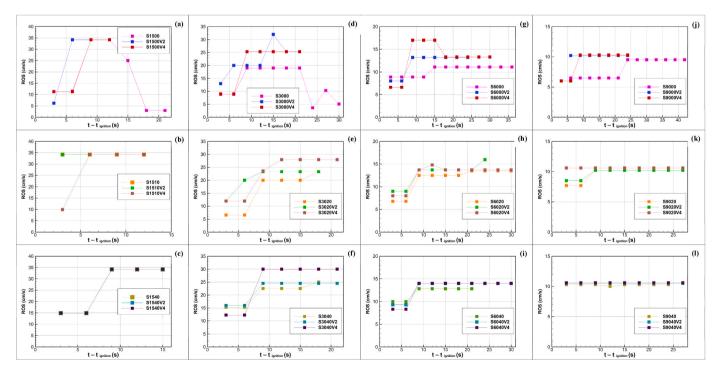**Fig. 8.** Time evolution of the ROS moving average (evaluated over a 3 s time interval) for $\theta = 15°$ (a–c), for $\theta = 30°$ (d–f), for $\theta = 60°$ (g–i), and for $\theta = 90°$ (j–l), and for different combinations of the slope angle and wind speed. Recall notation: S1520V2 corresponds to a simulation with $\theta = 15°$, $\alpha = 20°$, and $U = 2$ m/s.

(with 10° intervals), for junction angles of 15°, 30°, 60°, and 90°, and for two values of open wind speed: 2 and 4 m/s (in addition to no-wind condition). The following notation is used in the results section: Simulation S1520V2 corresponds to $\theta = 15°$, $\alpha = 20°$ and $U = 2$ m/s; when V# is omitted, the simulation corresponds to a no-wind case.

3. Results and discussion

3.1. Flow streamlines and temperature field

To analyse the behaviour of junction fires, the interaction of flow streamlines and the temperature field around the flame is represented for different wind speeds, terrain slope angles, and junction angles. Fire propagation for different combinations of the slope angle and wind speed are illustrated in Fig. 4 (for $\theta = 15°$) and 5 (for $\theta = 60°$). The streamlines reveal how fresh air is being drawn into the flaming zone and recirculation zones are clearly developed in no-wind cases, with and without a slope, as shown by subplots (a) and (c) of Figs. 4 and 5. In wind-driven conditions, the structure of the flow field is less affected by the fire, as shown in subplots (b) and (d), where a noticeable slant of the flames in the wind direction can be observed. The action of the fire on the overall flow field is in this case limited to the local vertical acceleration due to buoyancy. Figs. 4 and 5 show that similar temperature levels are obtained in the flaming zone for all considered cases, but a significantly large extent of the flaming zone is obtained for smaller junction angles for all the considered combinations of the slope angle and wind speed.

3.2. Propagation and ROS

In Figs. 6 and 7, the average junction point position was obtained in the median vertical plane from the average position of the pyrolysis front in the fuel bed thickness (as described in Hassan et al. [7]). The dynamic ROS was obtained from the time derivative of the average junction point position, using a simple 1st order forward differentiation at each time step of the simulation. The horizontal lines in Figs. 6 and 7 correspond to the average value of the ROS obtained over the entire fire spread. This average ROS would serve as a useful reference for assessing the effects of wind speed and other parameters on the overall junction fire behaviour, as it will be shown further on in the discussion. Globally, it can be noticed that fire propagation is highly dynamic, characterised by high variability in the dynamic ROS (with short timescale oscillations), intermittency in fire spread, and occasional fire jumps. Overall, fire is observed to spread in what might be called a surge-and-stall manner [17].

Recognising the need for a more refined and stable depiction of the ROS that still accounts for the unsteady nature of the phenomenon, a moving average of the ROS was evaluated from Figs. 6 and 7 over a 3s time interval. The resulting ROS values are shown in Fig. 8 for different junction angles and combinations of the slope angle and wind speed. Acceleration, quasi-steady and deceleration phases can be seen in this case. The junction effect can be clearly seen with an acceleration that increases as the junction angle decreases (i.e., as one moves from right to left in Fig. 8). For a junction angle $\theta = 15°$, the junction angle effect totally dominates the wind and slope effects, due to a strong interaction between the close fire lines which dominates all other external parameters. We note that the deceleration phase seen in S1500 (Fig. 8a) disappeared when the wind was applied.

For a junction angle $\theta = 15°$, the ROS values are close to identical for a slope angle $\alpha = 40°$ (Fig. 8c). This case corresponds to the maximum value of 34.5 cm/s obtained for the ROS moving average. Due to the combined effect of the junction and the slope, the wind effect was totally insignificant in this case (at least up to 4 m/s). For $\theta = 30°$ (Fig. 8d–f), the increasing effect of the wind on the ROS is clear for all slope angles. A deceleration phase is only observed for small junction angles in no-wind conditions (see Fig. 8a and d, see also Hassan et al. [7]), and it
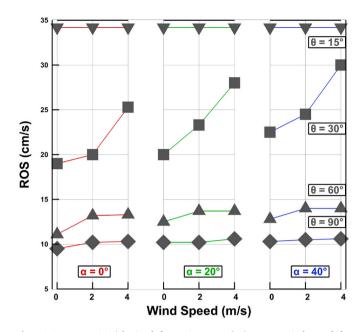

Fig. 9. Average ROS (obtained from Figs. 6 and 7) versus wind speed for different junction and slope. $\theta = 15°$ (▼), $\theta = 30°$ (■), $\theta = 60°$ (▲), and $\theta = 90°$ (◆). $\alpha = 0°$ (left), $\alpha = 20°$ (centre), $\alpha = 40°$ (right).

disappears when wind is applied.

Compared to a junction angle $\theta = 15°$, the ROS appears to be less influenced by wind speed for junction angles of 60° and 90° (Fig. 8g–l). For $\theta = 60°$, the increase of wind speed from 2 to 4 m/s did not noticeably influence the ROS for all slope angles, except for the initial fire establishment phase in no slope condition (Fig. 8g). For junction angles $\theta = 60°$ and 90°, wind accelerates fire establishment in the case of 0 and 20° slopes, i.e., the ROS reaches faster its final main value. For $\theta = 90°$ and $\alpha = 40°$ (Fig. 8l), the wind effect is practically absent.

In order to examine the effects of the junction angle, slope angle and wind speed on the overall fire propagation, the average ROS values are extracted from Figs. 6 and 7, and shown in Fig. 9. In agreement with the findings of previous works [7,9], the junction angle plays the most significant role in the junction ROS for prevailing wind speeds up to 4 m/s. The ROS dependence on the junction angle is not linear: for instance, for a wind speed of $U = 2$ m/s and slope angle $\alpha = 20°$, the average ROS decreases by about 14 cm/s when θ decreases from 15° to 30°, while it approximately drops by 4 cm/s when θ decreases from 60° to 90°. For small junction angles, junction effect (i.e., the interaction between the junction arms) dominates both slope and wind effects. Wind speed seems to have an important effect on junction fire propagation for intermediate values of the junction angle, as clearly shown in Fig. 9 for all slope angles. For large junction angles, wind seems to have less effect on junction fire propagation. Compared to the junction angle effect, the results also show that the slope angle has a weak effect on junction fire propagation, for all considered wind speeds.

3.3. Heat release rate (HRR)

In FIRESTAR3D, the total HRR is given by Eq. (1) where ω_{vap}, ω_{pyr}, ω_{char}, ω_{CO} and ω_{soot} are the total mass rates of water evaporation, pyrolysis, char combustion, combustion of CO in the gas mixture, and soot combustion, respectively; and ΔH_{vap}, ΔH_{pyr}, ΔH_{char}, ΔH_{CO} and ΔH_{soot} are the corresponding specific heats. Since vaporization and pyrolysis reactions are endothermic, they have negative contributions in Eq. (1). Note that ΔH_{char} is not constant in this case as it depends on the CO to CO_2 ratio produced during char combustion [8] (see also the paper appendix), it varies between 9 MJ/kg (for an incomplete combustion) and 30 MJ/kg (for a complete one).
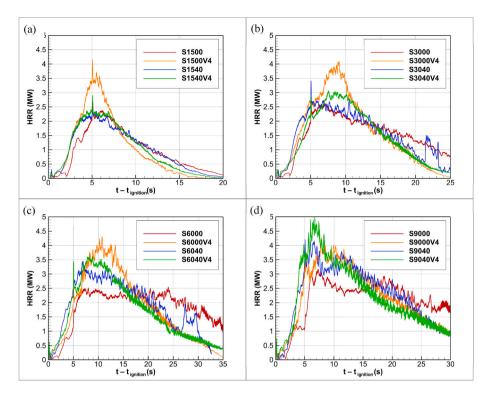
Fig. 10. Time evolution of HRR obtained for a junction angle of 15° (a), 30° (b), 60° (c), and 90° (d), with different combinations of the slope angle ($\alpha = 0$ and 40°) and wind speed ($U = 0$ and 4 m/s). Recall notation: S1520V2 stands for simulation with $\theta = 15°$, $\alpha = 20°$, and $U = 2$ m/s.

$$HRR = -\omega_{\text{vap}}.\Delta H_{vap} - \omega_{\text{pyr}}.\Delta H_{pyr} + \omega_{char}.\Delta H_{char} + \omega_{CO}.\Delta H_{CO}$$
$$+ \omega_{soot}.\Delta H_{soot} \qquad (1)$$

An important fire property related to the HRR is the fire intensity (W/m) defined as the HRR per unit length of the fire front. For a straight fire front, fire intensity (FI) can be related to the ROS by Eq. (2), where $W = \alpha_s \rho_s h$ (kg/m²) is the fuel load per unit area (h being the fuel height) and Δh_c (J/kg) is the heat of combustion of the fuel obtained from laboratory measurement.

$$FI = ROS \times W \times \Delta h_c \qquad (2)$$

From Eq. (2), fire intensity, and consequently the HRR, may be evaluated in the field. Another quantity related to the fire intensity or the HRR that can be measured in the field is the radiative heat flux received from a fire on a target. Good predictions of field measurements were obtained using FIRESTAR3D both for fire intensity and for the time evolution of the radiative heat flux received at several locations ahead of a fire front propagating on a sloped terrain [14].

Time evolutions of the HRR obtained in the case of junction fire are shown in Fig. 10 under different conditions. HRR time signals are characterised by high-frequency fluctuations resulting from flame intermittency due to the interaction with the local flow field. As shown in Fig. 10, the junction angle is again the main parameter affecting the time evolution of the HRR. Both the rise time (time to reach the maximum HRR) and the decline time decrease with the junction angle, i. e., junction fires are characterised by faster dynamics (thus more dangerous) for small junction angles. The HRR level (maximum and average) increases with the junction angle, which is mainly due to the fact that the length of the junction arms decreases faster as the junction angle decreases (recall that the HRR for a straight fire front is proportional to its length). It is also partially due to the fact that the amount of solid fuel increases with the junction angle for equal length of junction arms. Referring to Fig. 1, the amount of fuel increases 3.35 times when the junction angle increases from 15° to 60°, at equal lengths of junction arms. Fig. 10 also shows that the impact of the wind speed on the HRR
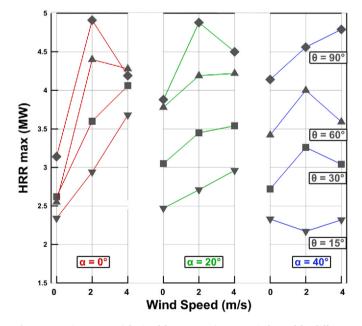

Fig. 11. Maximum HRR (obtained from Fig. 10) versus wind speed for different junction and slope angles. $\theta = 15°$ (▼), $\theta = 30°$ (■), $\theta = 60°$ (▲), and $\theta = 90°$ (◆). $\alpha = 0$ (left), $\alpha = 20°$ (centre), $\alpha = 40°$ (right).

decreases with the slope angle; indeed, wind speed substantially increases the HRR for $\alpha = 0$, while a slight increase is obtained for $\alpha = 40°$.

As in Fig. 9, the effects of the three parameters (junction angle, slope angle and wind speed) on the maximum HRR is summarised in Fig. 11, where, globally, the same conclusions drawn from Fig. 10 can be made. Fig. 11 shows a non-monotonic effect of the wind speed, where a higher HRR maximum was obtained at $U = 2$ m/s than at $U = 4$ m/s. This is due to the unsteady nature of the junction fire, where local maxima of the
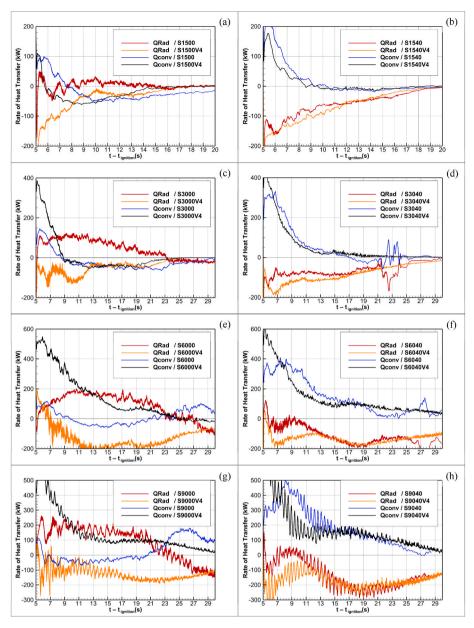
Fig. 12. Time evolution of convection and radiation heat transfer rates received by the solid fuel for two wind speeds (0 and 4 m/s). (a) $\theta = 15°$, $\alpha = 0°$; (b) $\theta = 15°$, $\alpha = 40°$; (c) $\theta = 30°$, $\alpha = 0°$; (d) $\theta = 30°$, $\alpha = 40°$; (e) $\theta = 60°$, $\alpha = 0°$; (f) $\theta = 60°$, $\alpha = 40°$; (g) $\theta = 90°$, $\alpha = 0°$; and (h) $\theta = 90°$, $\alpha = 40°$.

HRR may occur without being globally representative of the fire intensity.

3.4. Heat transfer mode

The density of heat transfer rate (W/m³) received by the solid fuel, resulting from convection heat exchange with the surrounding hot gases and from radiation heat exchange with the flames, is given by Eq. (3), where T is the temperature of the gas mixture, T_s is the solid-fuel temperature, α_s and σ_s are respectively the fuel volume fraction and surface-to-volume ratio (see Table 1), σ is Stephan-Boltzmann constant, and J is the total irradiance calculated by integrating the radiation intensity (obtained by solving the radiative transfer equation) in all directions [8]. The convection heat transfer coefficient is obtained from correlations that depend mainly on the shape of the fuel particles (cylindrical in this case) and local Reynold number [8].

$$\dot{Q} = h_s \alpha_s \sigma_s (T - T_s) + \frac{\alpha_s \sigma_s}{4} \left(J - 4\sigma T_s^4 \right) \qquad (3)$$

The rates of convection and radiation heat transfers received by the entire vegetation layer are obtained by integrating, respectively, the convective and radiative components of Eq. (3) over the entire solid-fuel volume. Time evolutions of the convection and radiation heat transfer rates obtained for junction fires are shown in Fig. 12 for different cases, where the junction angle increases from top to bottom, the four left subplots correspond to a zero slope, while the four right ones correspond to a 40° slope. We notice first that the rates of heat transfer globally increase with the junction angle (as shown by the vertical axis range). As for the HRR, this is mainly due to the fact that the length of the junction arms decreases faster as the junction angle decreases, and partially to the solid-fuel volume that increases with the junction angle. There is a significant difference between the left side (zero slope) and the right side (40° slope) of Fig. 12, which means that the slope angle is the most influencing parameter as far as the heat transfer modes are concerned.

In the case of a sloping terrain (right subplots), the solid fuel receives heat by convection (positive rate) and loses heat by radiation (negative rate), and wind speed enhances both rates (i.e., the solid fuel receives

more heat by convection and loses more heat by radiation). It should be noted here that, even when no wind is applied, convection is the main heat transfer mechanism in junction fire propagation on a sloping terrain due to fire-induced wind that brings fresh air into the flaming zone (as shown in Figs. 4 and 5) and heats up the vegetation ahead of the fire front. In the case of non-sloping terrain (left subplots in Fig. 12), when no wind is applied, flames are vertical and high (as shown in Figs. 5 and 6); consequently, radiation is the dominant mode of heat transfer driving junction fire propagation, while the vegetation mainly loses heat by convection. But when wind is applied, the roles played by radiation and convection are reversed, i.e., convection becomes the dominant mechanism of junction fire propagation, while the vegetation loses mainly heat by radiation.

4. General conclusion

The rate of fire spread and fire intensity can be severe in case of intersecting fire fronts and wind has a role in intensifying this extreme fire behaviour. In this study, the effect of a driving wind speed on junction fire behaviour (ROS and fire intensity) was numerically investigated at a laboratory scale (5-m junction arm's length) for different combinations of the junction and slope angles. A fully-physical multiphase CFD code (FIRESTAR3D) was used to conduct simulations for four junction angles (15°, 30°, 60° and 90°), for slope angles of 0, 20° and 40°, and wind speeds of 0, 2, and 4 m/s. It should be noted that under no-wind conditions, fire-induced wind occurs bringing fresh air from the open boundaries into the flaming zone.

Results showed that a junction fire it is highly dynamic, its propagation is characterised by a surge-and-stall like behaviour, with high variability in the ROS, intermittency in fire propagation, and occasional fire jumps. It is observed the junction angle has non-linear effect on fire behaviour (i.e., it gets stronger as the junction angle decreases) and fire intensity increases faster as the junction angle decreases, making the fire more surprising and dangerous for firefighters. For a small junction angle (mainly for $\theta = 15°$), the junction effect totally dominates and conceals wind and slope effects (for the considered range of these parameters), due to a strong interaction between the close fire lines. In the case of a large slope angle ($\alpha = 40°$), the wind effect was insignificant (at least up to 4 m/s) on the fire ROS and the HRR, due to the combined effect of the junction and the slope. For large junction angles ($\theta = 60°$ and 90°) and low slopes ($\alpha = 0$ and 20°), wind accelerates fire establishment and the ROS reaches its final average value faster. Wind effect seems to be most significant at intermediate junction angles (around 30°); this point is not yet fully understood and requires a more advanced analysis.

As far as the heat transfer modes are concerned, the slope angle seems to be the most influencing parameter. In the case of non-sloping terrain, radiation is the dominant mode of heat transfer driving junction fire propagation in the absence of a prevailing wind. When the velocity of the latter increases, convection becomes the dominant mechanism of junction fire propagation, while the vegetation mainly loses heat by radiation. In the case of sloping terrain, convection from the hot gases is always the driving mechanism of the junction fire propagation while heat is released from the hot fuel by radiation. In this case, wind speed enhances both heat transfer modes. Decreasing the junction angle increases the fire intensity and, consequently, intensifies both convection and radiation heat exchanges, but does not change their respective roles in junction fire propagation.

This study provided some insights into the potential roles played by the junction angle, slope angle, and wind speed during a junction fire. More advanced and detailed analysis is required to better understand the inherent interaction between the flaming zone and the flow field that determines the behaviour of the junction fire in different conditions, which can be best performed by numerical simulation. However, there is

a pressing need to conduct more laboratory and field experiments to gain a more detailed understanding of the underlying physics governing the behaviour of this extreme fire, as it directly impacts firefighter safety, evacuation planning, and resource allocation.

Declaration of competing interest

The authors declare that they have no known competing financial interests or personal relationships that could have appeared to influence the work reported in this paper.

Data availability

Data will be made available on request.

Appendix A. Supplementary data

Supplementary data to this article can be found online at https://doi.org/10.1016/j.firesaf.2023.104039.

References

[1] D. Strauss, L. Bednar, R. Mees, Do one percent of the forest fires cause ninety-nine percent of the damage? For. Sci. 35 (2) (1989) 319–328.
[2] K. Short, A spatial database of wildfires in the United States, 1992–2011, Earth Syst. Sci. Data 6 (2013) 297–366.
[3] J. Sharples, G. Cary, P. Fox-Hughes, S. Mooney, J. Evan, M. Fletcher, M. Fromm, P. Grierson, R. Mcrae, P. Baker, Natural hazards in Australia: extreme bushfire, Climatic Change 139 (2016) 85–99.
[4] D. Viegas, J. Raposo, D. Davim, C. Rossa, Study of the jump fire produced by the interaction of two oblique fire fronts. Part 1. Analytical model and validation with no-slope laboratory experiments, Int. J. Wildland Fire 21 (2012) 843–856.
[5] D. Viegas, J. Raposo, A. Figueiredo, Preliminary analysis of slope and fuel bed effect on jump behavior in forest fires, Procedia Eng. 62 (2013) 1032–1039.
[6] J. Raposo, D. Viegas, X. Xie, M. Almeida, A. Figueiredo, L. Porto, J. Sharples, Analysis of the physical processes associated with junction fires at laboratory and field scales, Int. J. Wildland Fire 27 (2018) 52–68.
[7] A. Hassan, G. Accary, D. Sutherland, K. Moinuddin, Physics-based modelling of junction fires: parametric study, Int. J. Wildland Fire 32 (2023) 336–350.
[8] D. Morvan, G. Accary, S. Meradji, N. Frangieh, O. Bessonov, A 3D physical model to study the behavior of vegetation fires at laboratory scale, Fire Saf. J. 101 (October 2018) 39–52.
[9] A. Hassan, G. Accary, D. Sutherland, K. Moinuddin, Physics-based Modelling of Junction Fires: Sensitivity and Validation Studies, Coimbra, 2022.
[10] A. Sullivan, W. Swedosh, R. Hurley, J. Sharples, J. Hilton, Investigation of the effects of interactions of intersecting oblique fire lines with and without wind in a combustion wind tunnel, Int. J. Wildland Fire 28 (2019) 704–719.
[11] A. Filkov, B. Cirulis, T. Penman, Quantifying merging fire behaviour phenomena using unmanned aerial vehicle technology, Int. J. Wildland Fire 30 (2021) 197–214.
[12] N. Frangieh, D. Morvan, S. Meradji, G. Accary, O. Bessonov, Numerical simulation of grassland fires behaviour using an implicit physical multiphase model, Fire Saf. J. 102 (2018) 37–47.
[13] N. Frangieh, G. Accary, D. Morvan, S. Meradji, O. Bessonov, Wildfires front dynamics: 3D structures and intensity at small and large scales, Combust. Flame 211 (2020) 54–67.
[14] J. Fayad, F. Morandini, G. Accary, F. Chatelon, C. Wandon, A. Burglin, L. Rossi, T. Marcelli, D. Cancellieri, V. Cancellieri, D. Morvan, S. Meradji, A. Pieri, G. Planelles, R. Costantini, P. Briot, J. Rossi, A study of two high intensity fires across Corsican shrubland, Atmosphere 14 (3) (2023) 473.
[15] J. Gilliers, W. Nickling, J. King, Drag coefficient and plant form response to wind speed in three plant species: burning Bush (Euonymus alatus), Colorado Blue Spruce (Picea pungens glauca.), and Fountain Grass (Pennisetum setaceum), J. Geophys. Res. 107 (D24) (2002) 4760.
[16] D. Morvan, Physical phenomena and length scales governing the behaviour of Wildfires: a Case for Physical Modelling, Fire Technol. 47 (2011) 437–460.
[17] J. Dold, A. Zinoviev, Fire eruption through intensity and spread rate interaction mediated, Combust. Theor. Model. 13 (5) (2009) 763–793.